Journal of Geophysical Research
August 2008; Volume 113 (C08040) : Pages 1-8
http://dx.doi.org/10.1029/2007JC004587

An edited version of this paper was published by AGU.

Iceberg detection in open water by altimeter waveform analysis

Jean Tournadre[1, *], Kirk Whitmer[1, 2], Fanny Girard-Ardhuin[1]

[1] IFREMER, Laboratoire d'Océanographie Spatiale, Plouzané, France.
[2] IFREMER, Laboratoire de Physique des Océans, Plouzané, France.

*: Corresponding author : Tournadre J., email address : jean.tournadre@ifremer.fr

Abstract:

Small icebergs (edge lengths <1 km) are difficult to detect and track. In a recently published study, it was demonstrated that small targets (ships, islets,…) emerging from the sea can be detected by the analysis of high-rate altimeter waveforms. The analysis of Jason altimeter data revealed that small icebergs also have a detectable signature in the thermal noise part of the altimeter waveforms for open water. These signatures are very similar to that of transponders and are almost deterministic. An automated method based on the detection of parabolic shapes in the thermal part of the waveforms by analysis of the convolution product with a filter has been developed and applied to 1 year of Jason high-rate waveform data. In addition, the minimum height and backscatter of the iceberg can also be estimated by this method. More than 8000 icebergs were identified between December 2004 and November 2005 in the open water around Antarctica. The annual distribution of icebergs presents a well-defined tripole structure, with maxima near the Antarctic Peninsula, the West Ice Shelf, and the Ross Sea. This distribution is in good agreement with the main trends in Antarctic iceberg motion presented in the scientific literature. The high concentration of icebergs propagating from the Antarctic Peninsula seems to confirm the importance of this region in the discharge of Antarctic ice into the ocean. The results clearly show that altimeter data are a powerful tool in the study of the distribution of small icebergs largely inaccessible by other satellite means. The principle of detection of icebergs by altimeter is quite simple and could be easily applied to the existing archive of all the past and present altimeters (ERS, Topex/Poseidon, Jason, and Envisat) to create a database covering more than 13 years that could improve our knowledge of climate change in Antarctica.

Keywords: Altimeter waveform; iceberg; Antarctica

1. Introduction

Small icebergs, typically smaller than 1 km2, are difficult to detect using satellite borne sensors. Visible and infrared sensors are often blinded by clouds, low resolution microwave sensors, such as radiometers and scatterometers, cannot detect such small features and Synthetic Aperture Radars, although their detecting capabilities have been demonstrated (Silva and Bigg [2005], Gladstone and Bigg [2002]) have yet to be used on an operational basis to produce iceberg distribution or climatology, mainly because of the large amount of data to process. Until now, radar altimeters have been used primarily to study ice sheets but no attempt has yet been made to use the full capabilities of the analysis of the altimeter high rate (20 Hz) waveforms. In a recent study, Tournadre et al. [2006] demonstrated that small targets emerging from the sea surface, such as lighthouses, ships and small islets, have a detectable signature in the thermal noise section of space-borne altimeter echo waveforms and can thus be detected and analyzed. The detectability of a target depends primarily on its altitude above the sea level. Small icebergs, at least in open water, should also produce such a signature and the analysis of Jason altimeter waveforms over the southern ocean confirms the presence of a large number of signatures of emerging features south of 50±S. These features are caused by icebergs whose size is of the order of 1 km2. Indeed, the backscatter associated with larger icebergs becomes large enough to significantly modify the altimeter waveform and especially to change the leading edge. Unfortunately, this rapid change of the mean surface elevation causes the altimeter tracker to loose lock and result in the loss of data.

The present study aims at demonstrating, firstly, the capability of radar altimetry to detect small icebergs within open water through the analysis of the high rate waveforms and to estimate at least crudely their height and surface, and secondly, the potential of such detection for climatological studies of the distribution of small icebergs, especially in the southern oceans. The detection of icebergs within sea ice by altimeter waveforms analysis might also be possible as shown by some nice examples of icebergs signatures in elevation measured by the Envisat Radar Altimeter in the Weddell Sea Lubin and Massom [2007]. However, the nature of altimeter echoes over sea ice is too different from the open water one to allow the definition of a common processing. The detection within sea ice is thus not considered in this study. The signature of icebergs in ocean altimeter waveforms is described in detail in Section 2 and an example of an iceberg detected in the Jason archive is presented and analyzed. The automated detection algorithm used to process the Jason altimeter archive data is presented in Section 3, as well as the iceberg parameters that can be inferred from this analysis. The results of the processing of one year of Jason data are then analyzed in section 4 in terms of frequency, height, and backscatter. Finally section 5 summarizes the results and presents the prospective for the processing of the archives of past and present altimeter mission data. 2. Signature of icebergs The CNES/NASA Jason mission was designed to ensure the continuity of the observation and monitoring of the ocean provided by Topex/Poseidon and it has basically the same characteristics. It was launched on December 7th, 2001. Its main instrument is the Poseidon-2 altimeter, which was derived from the experimental Poseidon-1 altimeter on board Topex/Poseidon. It is a compact, low-power, low mass instrument offering a high degree of reliability. The dual-frequency Poseidon-2 operates at the same frequencies as the Topex NRA altimeter, i.e. 13.6 GHz (Ku band) and 5.3 GHz (C band). Depending on the sea state, the altimeter footprint varies from 5 to 10 km radius. The satellite samples the ocean surface between 66±S and 66±N at a 1-s interval (corresponding to a

5.8 km ground distance) for each of the 254 passes that make up a 9.9156-day repeat cycle. A detailed description of the Poseidon-2 altimeter is given in *Ménard and Fu* [2001]. The main Jason altimeter and satellite characteristics are the following: altitude 1324 km, inclination 66^o, waveform frequency 20Hz, pulse repetition frequency 1800 Hz, number of waveforms on average 90 per 0.05 s, telemetry bin width 3.125 ns, nominal track point 32.5.

The backscatter coefficient of the echo waveform can be expressed as a double convolution product of the radar point target response, the flat sea surface response and the joint probability density function of slope and elevation of the sea surface (*Brown* [1977]). The radar cross section for backscatter as a function of time, $\sigma(t)$, assuming a Gaussian altimeter pulse and a Gaussian random distribution of rough-surface specular points, can be expressed as (*Barrick and Lipa* [1985])

$$\sigma(t) = \frac{1}{2}(2\pi)^{3/2} H'' \sigma_\tau \sigma_0 \left(1 + \mathrm{erf}\left(\frac{x}{\sqrt{2}\sigma_p}\right)\right) e^{-\frac{x}{u_b}} \quad (1)$$

where $x = ct/2$, $H'' = H/(1 + H/a)$ is the reduced satellite height, a being the earth's radius, and H the satellite height. σ_τ is the standard deviation of the altimeter pulse; $\sigma_p = \sqrt{h^2 + \sigma_\tau^2}$ where h is the rms wave height; u_b is the antenna pattern standard deviation; σ_0 is the target backscatter coefficient. It should be noted that $t = 0$ corresponds to the mean sea level. The measured waveforms are given in telemetry samples of 3.125 ns width (the length of the pulse) and the nominal track point (i.e. the sea level or t=0) is shifted to bin 32.5. In a computation similar to the one presented by *Denys et al.* [1995] and *Roca et al.* [2003] for transponders, it can be easily shown by simple geometry that a point target of height δ above sea level located at distance d from the satellite nadir will give an echo at the time t_0 defined by (*Powell et al.* [1993])

$$\frac{ct_0}{2} = -\delta + \frac{1}{2}\frac{a+H}{aH}d^2 = -\delta + \frac{d^2}{2H"} \quad (2)$$

The echo waveform of a point target is purely deterministic, i.e. a parabola as a function of time. Using the radar equation (*Roca et al.* [2003]) and assuming a Gaussian antenna pattern and altimeter pulse, it is of the form

$$\sigma_{target}(t) = \frac{\sigma_1}{2\pi^2 H^4 (1 + \frac{d^2}{2H^2})} e^{-\frac{u_0}{u_b}} e^{-\frac{(x+\delta-u_0)^2}{2\sigma_\tau^2}}, \quad (3)$$

where σ_1 is the target radar cross section, and $u_0 = \frac{d^2}{2H''}$.

For an iceberg of surface *A* and constant backscatter coefficient σ_1, the waveform is obtained by summation of (3) over *A*

$$\sigma_{ice}(t) = \frac{\sigma_1}{2\pi^2 H^4} \oint_A \frac{1}{1 + \frac{d^2}{2H^2}} e^{-\frac{u_0}{u_b}} e^{-\frac{(x+\delta-u_0)^2}{2\sigma_\tau^2}} dA \quad (4)$$

A first condition for an iceberg to be detectable in altimeter echo waveforms is that time, t_0, lies within the time range during which the echo waveform is integrated, i.e. for the telemetry samples between 1 and 30. Figure 1-a presents the value of the telemetry sample for different distances from nadir and iceberg heights. For example, a 10 m high iceberg can be seen at distances from nadir between 0 and 8 km. At the satellite nadir, the maximum height of an iceberg that can be detected is 15 m. Indeed, the signature of higher icebergs will arise before the first telemetry sample and can thus not be detected. This means that only icebergs with a draught less than about 100 m can be detected. A second necessary condition for detection is that the target backscatter coefficient must be large enough to come out of the background sea surface backscatter. The backscatter of a small iceberg depends on its distance from nadir and its area. Figure 1-b presents the maximums of σ_{ice} for icebergs from 0.01 to 1 km^2 and distance from nadir from 0 to 18 km assuming a constant backscatter of 12 dB . The backscatter rapidly increases with size and decreases with distance from nadir.

Figure 2 presents an example of a simple signature of icebergs in Ku band Jason waveforms. The parabola visible near 59.05°S is characteristic of the signature of a small target overflown by an altimeter. It is similar to a transponder echo and follows relation (2).

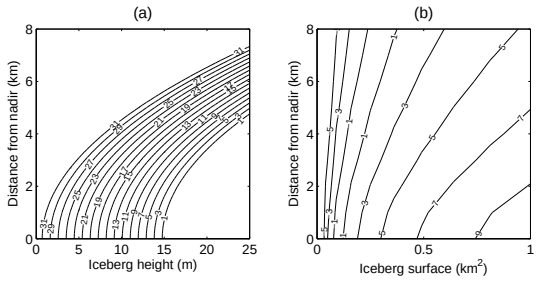

Figure 1. Detectability of an iceberg: (a) telemetry samples of the signature as a function of iceberg height and distance from nadir, (b) backscatter coefficient as a function of distance from nadir and surface assuming a 12 dB constant surface backscatter.

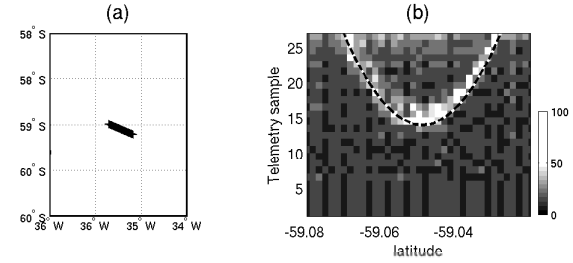

Figure 2. Iceberg signature detected near Antarctica on Jason cycle 143 pass 49 , November 25 2005. Geographical location (a), Ku band waveforms for telemetry samples 1 to 30 (thermal noise). The dashed line represents the best fit for a 8.5 m high iceberg located at the satellite nadir (b).

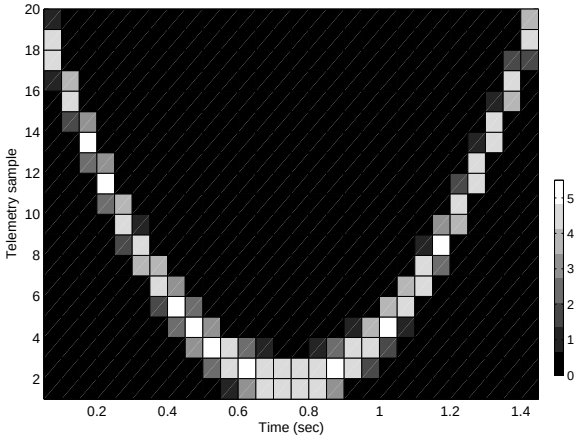

Figure 3. Filter used for the iceberg detection. The gray scale coding is given in arbitrary units.

Using the waveform model described by relation (4), the best fit of the Ku band observed waveforms was obtained for a 100 x 100 m^2 , 8.5 m high iceberg located on the satellite nadir at 59.05°S.

Some detected icebergs signatures are more complex that the simple example presented. Small groups of up to eight icebergs, separated by a few kilometers and having overlapping signatures, are quite regularly observed. They are most probably associated to the breaking up of larger icebergs. Some signatures are characterized by parabolas much wider than one waveform. They correspond to medium size icebergs whose characteristic length is about 1 km.

3. Icebergs detection

As the signature of icebergs is almost deterministic and always characterized by the parabolic shape defined by (2), an automated method of detection can be easily set up. The chosen method is based on the analysis of the convolution product C between a filter, F characteristic of an iceberg signature, and the thermal noise sections of the waveforms.

$$C(i,j) = \sum_{n=1}^{30} \sum_{m=1}^{M_2} \sigma_0(i,j) F(i-n, j-m) \qquad (5)$$

where i is the telemetry sample index, j, the waveform index, and $\sigma_0(i,j)$, the j^{th} waveform. The filter used, presented in Figure 3, has been computed by the waveform model of (4) for a 100x100 m^2 iceberg.

For each waveform, the maximum of correlation $C(j)$ and its location $i^C_{max}(j)$ are determined. The maximum of backscatter, $\sigma_{max}(j)$ and its location $i^\sigma_{max}(j)$ are also determined. A waveform is assumed to contain an iceberg signature if $C_{max}(j)$ and $\sigma_{max}(j)$ are larger than given thresholds C_1 and σ_1. These thresholds have been empirically determined by analysis of hundreds of iceberg signatures.

For each signature a maximum of 40 waveforms can be affected (this can easily be shown using relation (2)), if *n* consecutive waveforms are detected as containing a signature, the iceberg's parameters are determined as follows. The icebergs height, H_{ice}, is computed using (2) and assuming that the iceberg is located on the altimeter ground track, i.e. $d = 0$;

$$H_{ice} = (32.5 - \min(i^\sigma_{max}(j),\ j = 1..n)) * 0.4688 \qquad (6)$$

This height is in fact the minimum height of the iceberg because the distance from nadir is assumed to be zero. The iceberg mean backscatter, σ_{ice}, is estimated as the maximum observed backscatter of the whole signature, i.e.

$$\sigma_{ice} = max(\sigma_{max}(j),\ j = 1..n) \qquad (7)$$

As an illustration of the detection algorithm, figure 4-a presents the convolution product, *C*, between the filter, *F*, shown in figure 3, and the waveforms associated to an iceberg signature, presented in figure 2-b. The convolution greatly improves the signal to noise ratio of the iceberg signature against the thermal noise and facilitates the detection of the signature. The maxima of correlation, i^C_{max} , and of backscatter, i^σ_{max} determined by the detection algorithm are shown in figure 4-b as well as the final location of the iceberg signature.

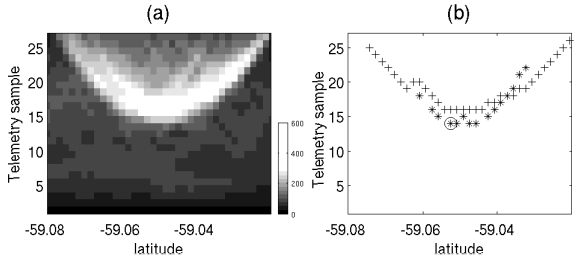

Figure 4. Detection of iceberg signature. Correlation between the observed waveform and the filter of figure 3 (a). Location of the maxima of correlation (crosses) and backscatter (star). The large circle indicates the sample selected by the detection algorithm (b).

4. Iceberg distribution

One year of Jason Ku and C-band waveforms from December 2004 to November 2005 (cycles 105 to 142) have been processed using the detection method to produce an iceberg database for the southern oceans. More than eight thousand signatures were detected in open water south of 45°S and analyzed. The number of icebergs detected each day, as presented in Figure 5, exhibits a strong seasonal cycle with a minimum during the austral winter and a maximum in February during the austral summer where nearly 100 icebergs are detected every day. This seasonal variation of the number of icebergs detected in open water is primarily correlated to the variation of the sea ice extent which is of course maximum in Winter. Figure 6-a presents the number of small icebergs detected on a 250x250km^2 regular polar stereographic grid. Because of the sampling pattern of the Jason altimeter, the number of altimeter data samples available in each grid cell is not homogeneous and is dependent on latitude. The number of detected icebergs has thus been normalized to take into account this under-sampling at lower latitudes. This is done by multiplying the number of icebergs by the inverse of the under-sampling, i.e. $Corr(i,j) = max(n(i,j))/n(i,j)$, where $n(i,j)$ is the number of Jason samples available at the *(i,j)* grid point. The geographically corrected distribution is presented in figure 6-b.

The iceberg's northern limit is in good agreement in all regions with northernmost limits from visual observations (*Soviet Antarctic Survey* [1966]) and iceberg trajectory modeling (*Gladstone et al.* [2001]). The geographical distribution exhibits a strong tri-pole structure, one maximum in each ocean. The southern Atlantic maximum extends from Graham Land to the west to the South Sandwich Islands to the east. It extends much further north of the maximum sea ice extent and reaches 50^{o}S near 10^{o}W. The structure of this maximum suggests a strong and mostly westward propagation of icebergs away from the Antarctic Peninsula. The pattern of the distribution in this region also indicates that the movement of one part of the iceberg field has a strong northward component which drives some of them as far north as 45^{o}S. As suggested by *Long et al.* [2002] the large number of small iceberg's observed in this

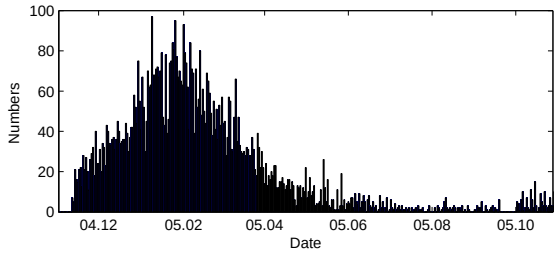

Figure 5. Number of icebergs detected each day by the Jason altimeter.

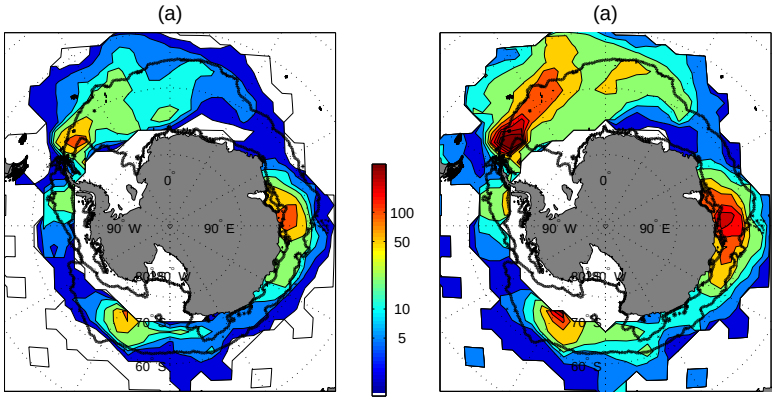

Figure 6. Number of icebergs detected in 250x250km^2 boxes from November 2004 to December 2005 (a). Number of icebergs detected normalized for the difference of Jason sampling as a function of latitude (b). The color scale is logarithmic. Solid black lines represent the maximal and minimal sea ice extent from AMSRE data from IFREMER/CERSAT data center.

region north of the Weddell sea might result from the calving of many small icebergs from large tabular icebergs which follow very repeatable patterns and generally end up in the Weddell Sea.

The second zone of high concentration is located in the south Indian Ocean near the West Ice Shelf (90^{o}E). It only extends to the north of the maximum sea ice limit over the Kerguelen Plateau (80^{o}E). The propagation appears limited to between the Amery Ice shelf (70^{o}E) and 120^{o}E. The third maximum is found in the Ross Sea. It is of quite small extent and concentrates near 150^{o}W. It is almost entirely contained within the maximum sea ice extent limit. Its shape suggests weak northward and westward transports. Finally, a secondary weaker maximum is observed in the Bellinghausen Sea (90^{o}W).

Three minima where almost no icebergs are detected are also well defined. In the south Indian Ocean off of Enderby Land (from 30^{o}E to 50^{o}E) less than 5 icebergs per grid box have been detected during the year. In the south Pacific near 90°W where the sea ice extent has very little annual variability a second minimum is observed, as well as a third in the western Pacific off the Terre Adélie.

The distributions of icebergs for the four seasons have also been computed and are presented in Figure 7. In winter, there are almost no icebergs in open water except for a few propagating off the Antarctic peninsula and off the West Ice Shelf. In spring, sea ice starts to melt over large regions releasing trapped icebergs. The maxima of concentration are observed in the four zones described earlier, especially near Graham Land and near the Denman and Scott glaciers. As the year progresses the sea ice retreats to reach its minimum at the end of summer and more icebergs are detected in open water. It is interesting to note that except for the South Atlantic Ocean very few icebergs are detected north of the maximum sea ice extent. During the fall, the sea ice extends again trapping icebergs and the number of detected icebergs decreases rapidly except in the South Atlantic Ocean where it still increases north of the maximum sea ice extent near 40^{o}W.

The general patterns of the distribution field are in good agreement with the main trends in Antarctic iceberg motion as described for example by *Tchernia and Jeannin* [1984] and the results of iceberg trajectory modeling of *Gladstone et al.* [2001]. The distribution is also in very good agreement with the suggestion that the discharge from the Antarctic ice sheet is drained through a small number of fast moving ice streams and outlet glaciers (*Bamber et al.* [2000], *Rignot and Thomas* [2002]). Our results also appear to confirm the importance of the western Weddell Sea as a major region of iceberg export into the open ocean. This is in good agreement with the iceberg drift in the Weddell Sea estimated from buoy data by *Schodlok et al.* [2006] and modeled by *Gladstone et al.* [2001], which showed that the circulation associated with the Weddell Gyre tends to export near the northeastern tip of the Antarctic Peninsula the icebergs originated from the Antarctic coast from the Antarctic Peninsula to the west to the Amery Ice Shelf to the east. The trajectories of small to medium sized icebergs tagged in the Weddell sea presented by *Schodlok et al.* [2006] confirm the strong northward component of the drift for icebergs originating in the western Weddell Sea as observed in the altimeter distribution. Some icebergs are detected north of 50^{o}N. The distribution pattern seems also to confirm the existence of two distinctive drift patterns east and west of 40^{o}W. West of this line, i.e. close to the Antarctic Peninsula, the elongated shape of the distribution maximum suggest a quite uniform northward/eastward component associated with the circumpolar current. East of 40^{o}W, the distribution is more uniform reflecting a more chaotic pattern of trajectories. This region is not only the major source of iceberg export within the open ocean but also the one associated with the largest northward transport. The structure of the second maximum iceberg concentration between 50°W and 140°W is also in good agreement with the distribution estimated from the Australian Antarctic Program's iceberg data set *Jacka and Giles* [2007].

The analysis of the iceberg's signature gives an estimate of the minimum height and backscatter of the icebergs. As the distance between an iceberg and the satellite ground track has an equiprobability, the median of the heights and backscatter of the iceberg detected over a given zone gives at least a rough estimates of the height and backscatter The median has been estimated on a 300x300km^2 regular grid and only the grid cells where more than 10 icebergs where detected have been kept. Due to the limited numbers of data in most of the grid cells (less than 50) the results must be analyzed with caution and are mainly given here as an illustration of the method. However, these parameters could be of interest for climate studies when analyzing their inter-annual variability on a lower resolution grid.

The median annual height presented in Figure 8 shows that the icebergs originating from the Antarctic Peninsula are higher than the ones from Eastern and Western Antarctica. Locally, for example near the Mertz Glacier (150°E), the height can also be larger. The icebergs that propagate the furthest are also on average higher; this is particularly obvious in the Southern Atlantic north of the maximum sea ice extent.

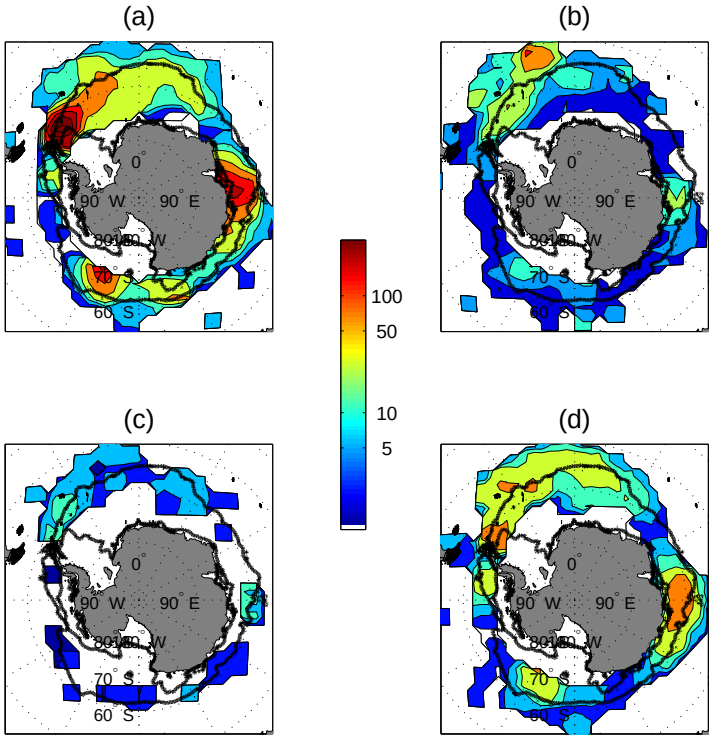

Figure 7. Normalized number of icebergs for January, February, March (austral summer) (a), April, May and June (austral Fall) (b), July, August and September (austral winter) (c) And October, November and December (austral spring) (d). The maximal and minimal sea ice extent are represented by solid black lines.

The mean backscatter is more complex to interpret as it depends not only on the distance from nadir and the surface of the iceberg, but also on the ice backscatter which can vary significantly depending on the ice roughness or the presence of liquid water. However, assuming that surface is, in a first order approximation, the main contributing term, the annual median field suggests that the Antarctic Peninsula icebergs are in the mean significantly smaller than the Eastern and Western Antarctica ones.

5. Conclusion and prospective

Small targets emerging from the sea surface have detectable signatures in high rate (20Hz) altimeter waveforms as already shown by *Tournadre et al.* [2006], as do small icebergs whose edge lengths are of the order of 1 km or less. The signature of icebergs is similar to that of transponders and is purely deterministic. An automated detection algorithm has thus been defined. It is based on the detection of coincident relative maxima of the backscatter and of the convolution product between the thermal noise part of the waveforms and a filter representing the theoretical signature of a point target. The detection is limited to open water and to icebergs that have less than 15m freeboard and within one kilometer size range. Icebergs outside of this range are thus not counted in the analysis. Within this range, the algorithm also allows the estimation of the minimum height of the icebergs and of its backscatter that can be seen in a first order approximation as a proxy of the iceberg surface. The processing of one year of Jason data revealed more than 8000 iceberg signatures south of 45°S in open water. The number of icebergs detected daily which can reach 100 in summer, is strongly correlated to the sea ice extent.

The annual distribution of icebergs presents a well-defined tripole structure with maxima near the Antarctic Peninsula, the West Ice Shelf and the Ross Sea. This distribution is in good agreement with the main trends in Antarctic icebergs motions presented in the literature and the results of trajectory modeling. The large concentration of icebergs exported into the open ocean off the Antarctic Peninsula seems to confirm the importance of this region in the discharge of Antarctic ice into the ocean. The height and backscatter estimates from the waveform analysis should be interpreted with caution as they also depend on the distance between the icebergs and the satellite ground track. However, their median distributions give at least a general idea of the characteristics of icebergs for the different regions. The icebergs originating from the Antarctic Peninsula are higher than the ones originating in the West Ice Shelf or in the Ross Sea, but their surfaces are smaller. These results need to be further confirmed by comparison, if possible with SAR and/or in situ data.

The results obtained for one year of data clearly show that altimeters are a powerful tool in the study of the distribution of small icebergs in the open ocean largely inaccessible by other satellite means. The principle of detection of icebergs with high rate altimeter waveforms is quite simple and could be applied to the existing archive of the past and present altimeters (ERS, Topex/Poseidon, Jason, Envisat) to create a database covering more than 13 years. This database could then be used for example to analyze the impact of climate change on the export of small icebergs in the open ocean, especially near the Antarctic Peninsula which experiences the largest warming in Antarctica (*Vaughan et al.* [2003]). In the future, it will also be of interest to study the possibility of a similar detection method using high rate altimeter waveforms over sea ice and to compare the results with those of SAR data analysis.

References

Bamber, J. L., D. G. Vaughan, and I. Joughin (2000), Widespread Complex Flow in the Interior of the Antarctic Ice Sheet, *Science*, *287*, 1248–1250.

Barrick, D., and B. Lipa (1985), Analysis and interpretation of altimeter sea echo, *Satellite Oceanic Remote Sensing, Advances in Geophysics*, *27*, 61–100.

Brown, G. S. (1977), The average impulse response of a rough surface and its applications, *IEEE Trans. Antennas Propag.*, *AP-25*, 67–74.

Denys, P. H., A. R. Birks, P. A. Cross, R. J. Powell, P. Pesec, and B. Burki (1995), Transponder altimetry precise height measurements over land, *J. Geophys. Res.*, *101*, 24.347–24.359.

Gladstone, R., and G. Bigg (2002), Satellite tracking of icebergs in the weddell sea, *Antarctic Science*, *14*, 278–287, doi: 10.1017/S0954102002000032.

Gladstone, R. M., G. R. Bigg, and K. W. Nicholls (2001), Iceberg trajectory modeling and meltwater injection in the Southern Ocean, *J. Geophys. Res.*, *106*, 19,903–19,916, doi:10.1029/2000JC000347.

Jacka, T. H., and A. B. Giles (2007), Antarctic iceberg distribution and dissolution from ship-based observations, *J. Glaciol.*, *53*, 341–356.

Long, D., J. Ballantyne, and C. Bertoia (2002), Is the number of icebergs really increasing, *EOS, Transactions of the American Geophysical Union*, *83 (43)*, 469 & 474.

Lubin, D., and R. Massom (2007), Remote sensing of earth's polar regions: Opportunities for computational science, *Computing in Science and Engineering*, *9*, 58–71.

Ménard, Y., and L. Fu (2001), Jason-1 mission, in *Aviso Newsletter*, vol. 8, AVISO Altimetry edition.

Powell, R. J., A. R. Birks, W. J. Wrench, and C. L. Biddiscombe (1993), Using transponders with ERS1-1 and Topex altimeters to measure orbit altitude to $\pm$ 3 cm, in *Proc. of First ERS- Symposium (ESA SP-359)*, pp. 511–516.

Rignot, E., and R. H. Thomas (2002), Mass Balance of Polar Ice Sheets, *Science*, *297*, 1502–1506, doi:10.1126/science.1073888.

Roca, M., H. Jackson, and C. Celani (2003), RA-2 sigma-0 absolute calibration, in *Proc. of Envisat Validation Workshop (ESA SP-531)*, p. 16 pp.

Schodlok, M. P., H. H. Hellmer, G. Rohardt, and E. Fahrbach (2006), Weddell sea iceberg drift: Five years of observations, *J. Geophys. Res.*, *111*, C06,018, doi:10.1029/2004JC002661.

Silva, T., and G. Bigg (2005), Computer-based identification and tracking of antarctic icebergs in sar images, *Remote Sensing of Environment*, *94*, 287–297, doi:10.1016/j.rse.2004.10.002.

Soviet Antarctic Survey (1966), *Antarctic Atlas*, Soviet Antarctic Survey, Moscow.

Tchernia, P., and P. F. Jeannin (1984), Circulation in antarctic waters as revealed by icebergs tracks 1972-1983, *Pola Rec.*, *22*, 263–269.

Tournadre, J., B. Chapron, N. Reul, and D. C. Vandemark (2006), A satellite altimeter model for ocean slick detection, *J. Geophys. Res.*, *111*(C4), C04,004, doi:10.1029/2005JC003109.

Vaughan, D. G., G. J. Marshall, W. M. Connolley, C. Parkinson, R. Mulvaney, D. A. Hodgson, J. C. King, C. J. Pudsey, and J. Turner (2003), Recent rapid regional climate warming on the antarctic peninsula, *Climatic Change*, *60*, 243– 274, doi:10.1023/A:1026021217991.

Tournadre Jean, Laboratoire d'Océanographie Spatiale, Ifremer, Technopôle de la Pointe du Diable, 29280, Plouzané, France (jean.tournadre@ifremer.fr)

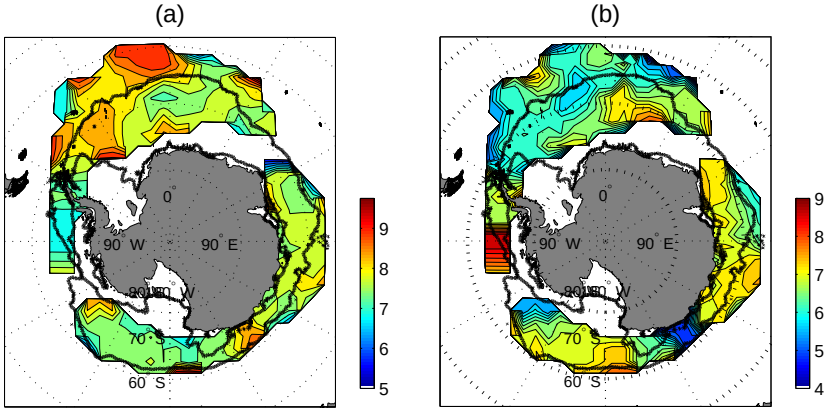

Figure 8. Median annual iceberg height in meters (a), and backscatter in dB (b). The maximal and minimal sea ice extents are represented by solid black lines.